

Article

Nano-Assemblies from J-Aggregated Dyes: A Stimuli-Responsive Tool Applicable to Living Systems

Meihui Su, Shuoxin Li, Hao Zhang, Junqing Zhang, Haoliang Chen, and Changhua Li

J. Am. Chem. Soc., **Just Accepted Manuscript** • DOI: 10.1021/jacs.8b10396 • Publication Date (Web): 14 Dec 2018

Downloaded from <http://pubs.acs.org> on December 14, 2018

Just Accepted

“Just Accepted” manuscripts have been peer-reviewed and accepted for publication. They are posted online prior to technical editing, formatting for publication and author proofing. The American Chemical Society provides “Just Accepted” as a service to the research community to expedite the dissemination of scientific material as soon as possible after acceptance. “Just Accepted” manuscripts appear in full in PDF format accompanied by an HTML abstract. “Just Accepted” manuscripts have been fully peer reviewed, but should not be considered the official version of record. They are citable by the Digital Object Identifier (DOI®). “Just Accepted” is an optional service offered to authors. Therefore, the “Just Accepted” Web site may not include all articles that will be published in the journal. After a manuscript is technically edited and formatted, it will be removed from the “Just Accepted” Web site and published as an ASAP article. Note that technical editing may introduce minor changes to the manuscript text and/or graphics which could affect content, and all legal disclaimers and ethical guidelines that apply to the journal pertain. ACS cannot be held responsible for errors or consequences arising from the use of information contained in these “Just Accepted” manuscripts.



Nano-Assemblies from J-Aggregated Dyes: A Stimuli-Responsive Tool Applicable to Living Systems

Meihui Su^{1,2}, Shuoxin Li^{1,2}, Hao Zhang¹, Junqing Zhang^{1,2}, Haoliang Chen^{1,2}, and Changhua Li^{1,2,3*}

¹State Key Laboratory of Medicinal Chemical Biology, Nankai University, Tianjin 300071, P. R. China. ²College of Pharmacy, Nankai University, Tianjin 300071, P. R. China. ³Key Laboratory of Functional Polymer Materials of Ministry of Education, Nankai University, Tianjin 300071, P. R. China.

ABSTRACT: Controlling the packing arrangements of dyes is a facile way of tuning their photophysical and/or photochemical properties, thus enabling new sensing mechanisms for photofunctional tools. Here, we present a general and robust strategy toward water-stable J-aggregated dye templated nano-assemblies by incorporating an amphiphilic diblock copolymer and a stimuli-responsive dye as the only two building components. An iodo-substituted boron dipyrromethene (BODIPY) was adopted as a template to direct the self-assembly of poly(ethylene glycol)-block-polycaprolactone (PEG-PCL), forming a core-shell nanoplate with slip-stacked BODIPYs as core surrounded by hydrophilic PEG shell. The self-assembled nanoplate is stable in cell culture medium and possesses a built-in stimuli-responsiveness that arises from BODIPY bearing *meso*-carboxylate protecting group, which is efficiently removed upon treatment with peroxyntirite. The resulting negative charges lead to rearrangement of dyes from J-stacking to non-stacking, which activates photoinduced singlet oxygen production from the nano-assemblies. The stimuli-activatable photosensitivity has been exploited for specific photodynamic ablation of activated RAW 264.7 cells with excessive endogenous peroxyntirite. In light of the generality of the sensing mechanism, the concept described herein will significantly expand the palette of design principles to develop diverse photofunctional tools for biological research and clinical needs.

■ INTRODUCTION

Dye assemblies with high packing orders possess novel optical or electronic functionalities relative to individual dye molecules.¹⁻²² Thus, controlling the packing arrangement of dyes would be a facile way of tuning photophysical and/or photochemical properties of dyes and thereby enabling new design principles for photofunctional tools including fluorogenic probes,²³⁻³¹ ratiometric photoacoustic probes,³²⁻³⁴ or activatable photosensitizers,³⁵⁻⁴⁵ among others. However, dye assemblies with sensing capabilities or activatable photofunctions toward biorelated species in living systems based on stimuli-triggered dye rearrangement face a demanding set of performance requirements, including stability in cell culture media, rapid response to specific species at acceptable low concentrations, and chemical flexibility (available for a diverse range of biorelated species). Herein, we present a versatile and robust strategy toward water-stable J-aggregated dye doped nano-assemblies with photophysical responses toward external stimuli through dye-templated self-assembly of amphiphilic copolymers. The mechanism of stimuli-responsive photophysical changes is based on the dye rearrangement within nano-assemblies driven by the stimuli-triggered hydrophobic to ionic conversion of dyes.

A representative slip-stacked dye containing nano-assembly was engineered by incorporating a peroxyntirite-responsive iodo-substituted BODIPY dye (**BD-PG_{Me}**; Figure 1a) and an amphiphilic diblock copolymer poly(ethylene glycol)-block-polycaprolactone (PEG-PCL_n, denoted as **P_n**; Figure 1b) as two building components. As summarized in Figure 1c, for **P_n** with short hydrophobic PCL segment (e.g., **P₈**) possessing weak self-

association, **BD-PG_{Me}** forms J-aggregate and serves as template to direct the self-assembly of **P₈**, leading to a core-shell nanoplate of **BD-PG_{Me}/P₈** with J-aggregated **BD-PG_{Me}** as core surrounded by **P₈** shell. Whereas for the **P_n** with longer PCL segments (e.g., **P₈₀**) possessing strong hydrophobic interactions with one another, they tend to form micelles and encapsulate **BD-PG_{Me}** inside the hydrophobic core in a random packing arrangement. Upon incubation of **BD-PG_{Me}/P₈** nanoplates with peroxyntirite, a fast rearrangement of BODIPY dyes from highly ordered J-stacking to non-stacking was established, with a structural reorganization also taking place in which nanoplates were converted into nanorods. As discussed below, capability in generating singlet oxygen upon photoirradiation, i.e., photosensitivity, of **BD-PG_{Me}/P₈** nanoplates, was inhibited in the slip-stacked arrangement and could be selectively switched on in response to peroxyntirite, owing to the dye rearrangement. Distinguished from most conventional optical sensing mechanisms including Förster resonance energy transfer (FRET),^{46,47} photo-induced electron transfer (PeT),⁴⁸ and intramolecular charge transfer (ICT),⁴⁹ to name a few, the sensing mechanism presented here is based on the chemical structural change induced dye rearrangement, thus expanding the palette of design principles to develop diverse photofunctional tools for biological research and clinical needs by adopting various dyes with desired photofunctions as self-assembly templates. Moreover, the synthesis of carboxyl-caged dyes is flexible, thus allowing the customization of dye-templates with sensitivity toward a wide range of biorelated species of interest via introducing specific triggering motifs.

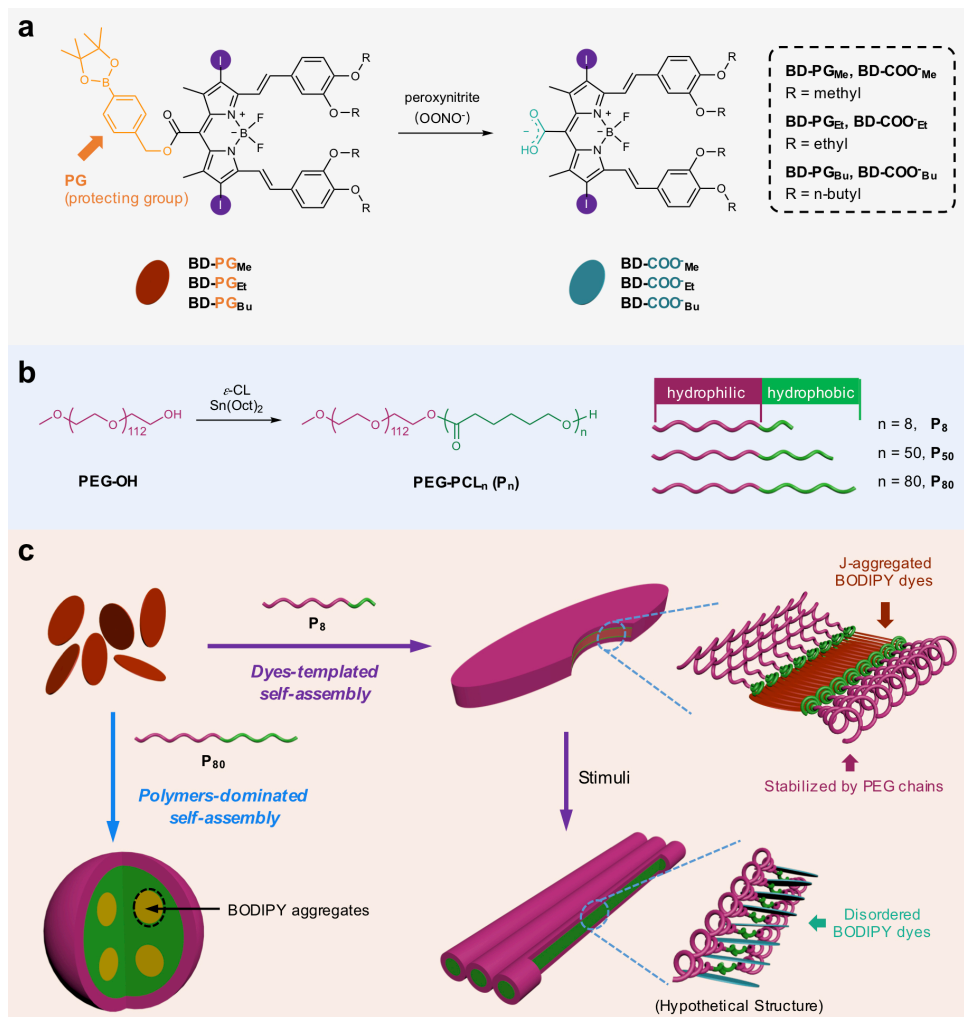


Figure 1. Representation of templated self-assembly and stimuli-triggered structure rearrangement, and chemical structures of two building components. (a) Chemical structures of three carboxyl-caged BODIPY dyes (**BD-PG_{Me}**, **BD-PG_{Et}**, and **BD-PG_{Bu}**), and stimuli-triggered deprotection chemistry. (b) Synthesis of amphiphilic diblock copolymer PEG-PCL_n (P_n) with different lengths of hydrophobic PCL segments. (c) Schematic depiction of engineering water-stable nanoplate with slip-stacked dyes as core surrounded by hydrophilic polymeric shell through dye templated self-assembly by incorporating an amphiphilic diblock copolymer and a hydrophobic dye as the only two building components. Stimuli-triggered shape transformation of nano-assemblies and concomitant rearrangement of dyes from J-stacking to non-stacking resulted in remarkable photophysical and/or photochemical changes.

RESULTS AND DISCUSSION

Core-shell nanoplate with J-aggregated dyes as core stabilized by polymeric shell. A key to this new type of self-assembled core-shell nanoplates with J-aggregated dyes as cores lies in the molecular design of hydrophobic BODIPY dyes, **BD-PG_{Me}** (Figure 1a), and amphiphilic diblock copolymer **P_n** (Figure 1b). **BD-PG_{Me}** bears a large benzyl ester moiety at the meso-position and two heavy iodine atoms at the 2,6-positions, which may be effective in preventing close face-to-face π -stacking while facilitating J-stacking of BODIPY dyes.^{9,50-53} Moreover, the meso-ester groups of **BD-PG_{Me}** are designed with the capability of stimuli-triggered hydrophobic ester to ionic carboxylate conversion, with the aim of providing an additional feature in actuating rearrangement of slip-stacked BODIPY dyes (Figure 1a). In organic solvents, such as DMSO, **BD-PG_{Me}** displayed an absorption band ranging from 550 to 780 nm with an absorption maximum (λ_{\max}) at 708 nm (Figure 2a), comparable

to those of other 2,6-iodo-substituted BODIPY dyes.⁹ Upon increasing the water content in the DMSO solution to a critical point (i.e., 30% water in DMSO, v/v), an explicit absorption band emerged at ca. 808 nm, indicating the formation of J-aggregates of **BD-PG_{Me}** (Figures 2a and S1).^{6,9} Although lack of hydrophilic groups, the J-aggregates formed in DMSO/water at higher water fractions (e.g., 90%) were demonstrated to be stable (Fig. S2). To explore such J-aggregates for potential applications in living systems, we propose to establish a platform for preparing water-based J-aggregates doped nano-assemblies via dye-assembly templated self-assembly of amphiphilic diblock copolymers (Figure 1c). Having no pendent group on the main chain, biocompatible amphiphilic diblock copolymer PEG-PCL_n (P_n) was selected as building block to minimize the interference of polymer on the packing arrangement and/or rearrangement of BODIPY dyes. Moreover, P_n with different hydrophobic PCL lengths could be prepared in a facile fashion by controlling the feed ratio of the ring-opening polymerization (Figure 1b). In this work, P₈, P₅₀, and P₈₀ with degrees of

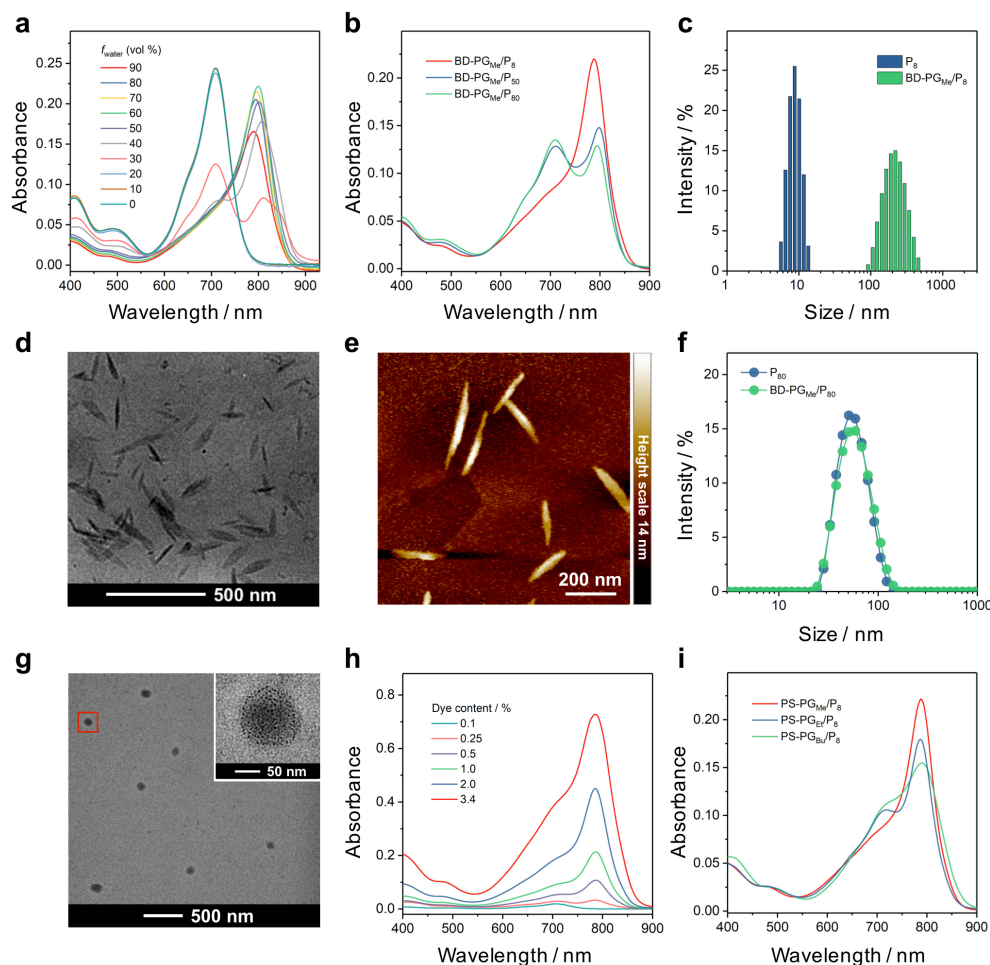


Figure 2. BODIPY dyes templated self-assemblies and their photophysical properties. (a) UV-visible absorption spectra of **BD-PG_{Me}** (4.0 μ M) in DMSO/water mixture with different water fraction (f_{water}) from 0 to 90% (vol %). (b) UV-visible absorption spectra of the aqueous solutions of **BD-PG_{Me}/P₈**, **BD-PG_{Me}/P₅₀**, and **BD-PG_{Me}/P₈₀** nano-assemblies. Conc. 4.0 μ M **BD-PG_{Me}**; 0.2 g/L **P_n**. (c) Size distribution of aqueous solutions of **P₈** (steel blue) and **BD-PG_{Me}/P₈** nano-assemblies (green) determined by DLS. (d) TEM image and (e) AFM image of **BD-PG_{Me}/P₈** nano-assemblies at 2.0% dye content. (f) Size distribution of aqueous solutions of **P₈₀** (steel blue) and **BD-PG_{Me}/P₈₀** nano-assemblies (green) determined by DLS. (g) TEM image of **BD-PG_{Me}/P₈₀** nano-assemblies at 2.0% dye content; inset shows a high magnification TEM image of the region marked with a red rectangle. (h) UV-visible absorption spectra of aqueous solutions of **BD-PG_{Me}/P₈** (0.4 g/L **P₈**) with different dye contents (0.1-3.4%). (i) UV-visible absorption spectra of the aqueous solutions of **BD-PG_{Me}/P₈**, **BD-PG_{Et}/P₈**, and **BD-PG_{Bu}/P₈** nano-assemblies. Conc. 4.0 μ M **BD-PG_R**; 0.2 g/L **P₈**.

polymerization (DP) of PCL segments of 8, 50, and 80, respectively, were prepared.

The nano-assemblies of **BD-PG_{Me}/P_n** through templated self-assembly using **BD-PG_{Me}** and **P_n** (**P₈**, **P₅₀**, and **P₈₀**) as two building components were prepared by slowly adding water to an acetone solution of **BD-PG_{Me}** and **P_n** over a period of 10 min to yield a final concentration of 0.4 g/L **P_n** and 8.0 μ M **BD-PG_{Me}** with dye content of 2.0%. Photophysical properties of the three different **BD-PG_{Me}/P_n** nano-assemblies were first investigated. Gratifyingly, remarkable bathochromic shifted absorption bands with λ_{max} at ca. 788 nm were observed for all three of the solutions, indicating the formation of J-aggregates (Figure 2b). However, differences in the absorption spectra of **BD-PG_{Me}/P₈**, **BD-PG_{Me}/P₅₀**, and **BD-PG_{Me}/P₈₀** solutions were observed. Regarding the **BD-PG_{Me}/P₈** solution, the monomer band at 708 nm almost disappeared, whereas for the other two solutions, residual monomer bands could still be observed to some extent. The fraction of J-aggregated **BD-PG_{Me}** dyes (α_1) was estimated from the apparent absorption coefficients (see Supporting Information), suggesting that the length of hydrophobic segments

has a significant impact on the dye arrangement (Figure S5). The variations in the absorption spectra suggest subtle differences in the arrangement of **BD-PG_{Me}** dyes, as well as the microscopic structures of three **BD-PG_{Me}/P_n** nano-assemblies. We then focused our attention to gain insights into the microscopic structures of the species generated from the self-assembly of **BD-PG_{Me}** and **P_n**. Surface tensiometer measurements of aqueous solutions of **P₈**, **P₅₀**, and **P₈₀** at 25 $^{\circ}$ C produced critical micelle concentrations (CMC) of 0.48, 0.06, and 0.02 g/L, respectively (Table 1). The relative high CMC of **P₈** was ascribed to its short hydrophobic PCL block, resulting in little driving force for micelle formation. Dynamic light scattering (DLS) measurements of aqueous solutions of **P₈**, **P₅₀**, and **P₈₀** at 0.1 g/L revealed intensity-average hydrodynamic diameters of 8, 45, and 60 nm, respectively (Table 1, Figures 2c, 2f, and S6), indicating that **P₈** was present as a unimer, whereas **P₅₀** and **P₈₀** formed micelles at the concentration used.

Table 1. Self-assembly properties of P_n in water with or without $BD-PG_{Me}$ dyes

Sample	CMC ^a / g/L	Size ^b / nm	PDI ^b
P_8	0.48	8.38 ^b	0.18
P_{50}	0.06	44.21 ^b	0.07
P_{80}	0.02	58.29 ^b	0.15
$BD-PG_{Me}/P_8$	/	~200 ^c	/
$BD-PG_{Me}/P_{50}$	/	59.71 ^b	0.13
$BD-PG_{Me}/P_{80}$	/	60.84 ^b	0.19

^aDetermined by surface tension analysis. ^bDetermined by dynamic light scattering (DLS) analysis. ^cThe length of the nanoplates was determined by atomic force microscopy (AFM) measurement. The results represent the average of three independent experiments.

We deduced that the weak self-association of P_8 in water could allow for dye assembly templated self-assembly in the presence of $BD-PG_{Me}$ dyes through hydrophobic interaction between $BD-PG_{Me}$ and P_8 (Figure 1c). Compared with unimer P_8 , the presence of $BD-PG_{Me}$ dyes induced an explicit increase in hydrodynamic diameters (Figure 2c), suggesting the formation of $BD-PG_{Me}/P_8$ nano-assemblies. The morphology and size of the nano-assemblies was investigated by transmission electron microscopy (TEM) and atomic force microscopy (AFM), and elliptical nanoplates with length over 200 nm and thickness approximately 10 nm were observed (Figures 2d and 2e). On the basis of DLS, TEM, and AFM results, together with UV-visible absorption studies (Figure 2b), we reasoned that $BD-PG_{Me}$ dyes were assembled in a slipped fashion in water and that the formed J-aggregates templated the self-assembly of P_8 , leading to the formation of $BD-PG_{Me}/P_8$ nanoplates via hydrophobic interaction between the PCL blocks of P_8 and J-aggregated $BD-PG_{Me}$ dyes as illustrated in Figure 1c. The formed J-aggregates doped $BD-PG_{Me}/P_8$ nanoplates were quite stable to dilution with negligible change in UV-visible absorption spectra following five 2-fold serial dilutions with phosphate buffered saline (PBS; Figure S7). The nano-assemblies were also demonstrated to be very stable in cell culture medium, or in saline with a sodium chloride concentration of 9.0% (w/v), which is 10 times that of physiological saline (0.90%, w/v; Figures S8 and S9). In the case of $BD-PG_{Me}/P_{80}$, the strong hydrophobic interaction between PCL segments was more favorable to the formation of micelles with dye aggregates entrapped within the hydrophobic core (Figure 1c). The size of $BD-PG_{Me}/P_{80}$ aggregates was slightly increased by 2.5 nm compared to that of P_{80} alone (Table 1 and Figure 2f), indicating little impact of $BD-PG_{Me}$ dyes on the self-assembly of P_{80} . TEM images revealed discrete nanoparticles with a size of approximately 70 nm for $BD-PG_{Me}/P_{80}$, as shown in Figure 2g. At higher magnification, darkened dots with sizes of 3-5 nm were observed throughout the nanoparticle due to localized aggregated $BD-PG_{Me}$ dyes (inset, Figure 2g); both monomer and J-bands were displayed (Figure 2b), demonstrating that $BD-PG_{Me}$ dyes were entrapped within the hydrophobic core in both slip- and non-stacked arrangements.

To assess the impact of the dye content on the templated self-assembly, several $BD-PG_{Me}/P_8$ solutions (0.4 g/L P_8) with different dye contents from 0.1% to 3.4% were prepared. With regard to $BD-PG_{Me}/P_8$ with low dye content (e.g., 0.1%), only a monomer band was observed in the UV-visible absorption spectrum (Figure 2h), suggesting that $BD-PG_{Me}$ dyes existed in a non-stacked arrangement, which should be attributed to the ex-

cessive P_8 chains that interfere with the π - π stacking and hydrophobic interaction between $BD-PG_{Me}$ dyes. Upon increasing dye content, the J-band at 788 nm emerged with the decrease of monomer band, indicating the formation of J-aggregates (Figure 2h). However, during the preparation of $BD-PG_{Me}/P_8$ nano-assemblies with dye content up to 4.0%, precipitation of dye aggregates was observed, and the actual dye content of the filtered solution was corrected to 3.4%, which is the maximum dye content of $BD-PG_{Me}/P_8$ nano-assemblies for which the J-aggregated $BD-PG_{Me}$ dyes could be well stabilized by P_8 . A plausible rationale for the instability of J-aggregates at high dye content is that the J-aggregates of BODIPY dyes should be stabilized by the surrounding hydrophilic PEG chains of P_8 , which are insufficient in the case of dye content beyond 3.4%. A plot of fraction of J-aggregated dyes (α_j) versus dye content suggested that $BD-PG_{Me}$ dyes in the slip-stacked arrangement were maximal with dye content in the range of 1.0-2.0% (Figure S10). Considering that the alkyl chains of BODIPY dyes might affect the intermolecular packing mode and self-assembly, $BD-PG_{Et}$ and $BD-PG_{Bu}$ with ethyl and n-butyl chains, respectively, were synthesized (Figure 1a). Upon increasing alkyl chain length from methyl ($BD-PG_{Me}$) to ethyl ($BD-PG_{Et}$) and n-butyl ($BD-PG_{Bu}$), significant changes in absorption spectra of $BD-PG_R/P_8$ nano-assemblies were observed (Figure 2i). Closer examination revealed that the fraction of J-aggregated dyes (α_j) decreased in the order of $BD-PG_{Me} > BD-PG_{Et} > BD-PG_{Bu}$ (Figure S11), presumably because long alkyl chains would interfere with π - π stacking interactions between dyes and enhance hydrophobic interactions between dyes and polymers. Collectively, the above results revealed that the J-aggregate templated self-assembly mechanism is governed by the subtle balance of non-covalent interactions including the self-association of PCL chains, π - π stacking and hydrophobic interactions between BODIPY dyes, and the hydrophobic interaction between PCL chains and BODIPY dyes.

Stimuli-triggered dye rearrangement within nano-assemblies. Having established that stable core-shell $BD-PG_{Me}/P_8$ nanoplates with J-aggregated $BD-PG_{Me}$ dyes as cores can be readily prepared in water by mixing P_8 and $BD-PG_{Me}$ following a templated self-assembly strategy, developing useful responsive outputs from the water-based J-aggregates would enable additional features and functions that promote promising applications in living systems. Since the caged-ester group at the *meso*-position of $BD-PG_{Me}$ is capable of stimuli-triggered hydrophobic ester-to-ionic carboxylate conversion via self-immolative chemistry, according to our previous report (Figure 1a),³¹ it could be anticipated that the generated negative charges of $BD-PG_{Me}$ units would disrupt or remodel the packing arrangement of $BD-PG_{Me}$ aggregates (Figure 1c), thereby inducing the photophysical and/or photochemical changes of the entire nano-assembly. Possessing arylboronate as a protecting group, $BD-PG_{Me}$ could be converted to *meso*-COOH-substituted $BD-COO_{Me}$ in the presence of peroxyxynitrite ($OONO^\cdot$),⁵⁴ as evidenced by a remarkable blueshift in the UV-visible absorption spectra (Figure 3a). HPLC analysis and high resolution mass spectrometry (HRMS) of the assay solution further confirmed the complete conversion from $BD-PG_{Me}$ to $BD-COO_{Me}$ in the presence of $OONO^\cdot$ as shown in Figure 3b and Figure S57, respectively. These preliminary results suggested that the iodine substituents at the 2 and 6 positions did not affect the stimuli-responsive feature of *meso*-ester-BODIPY dyes.

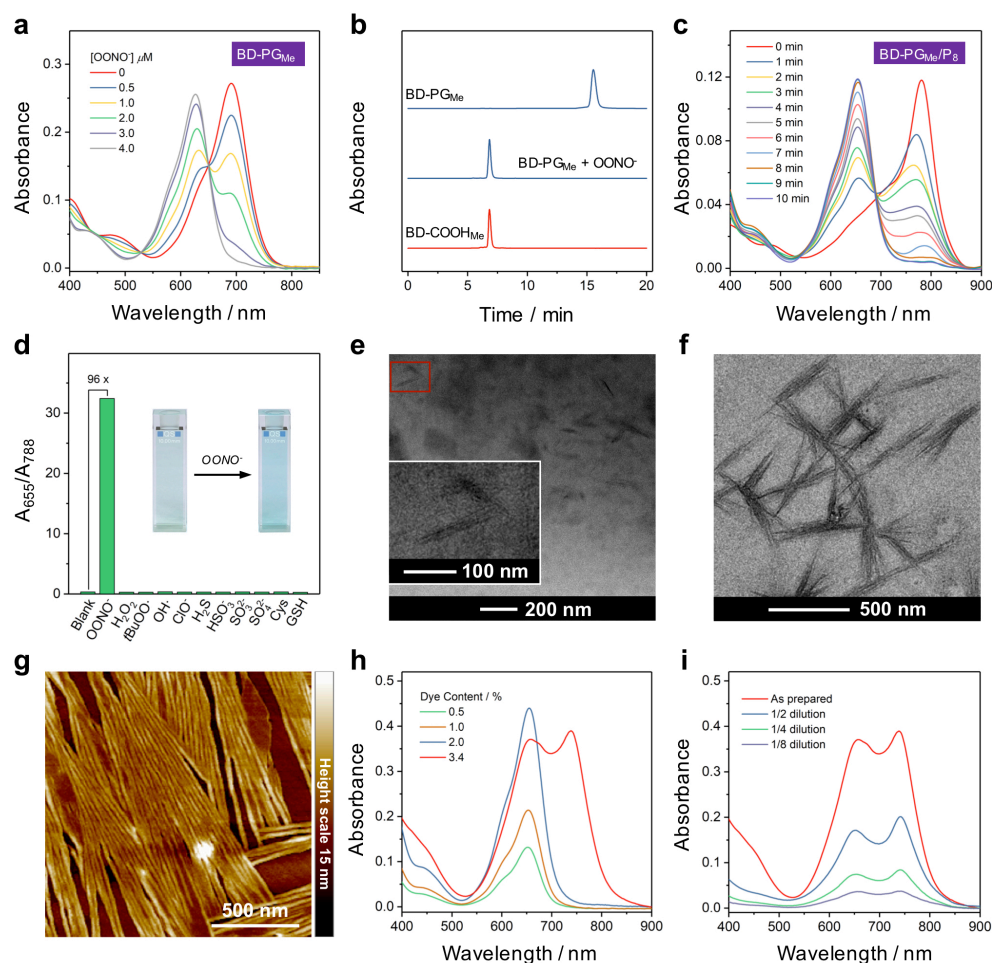


Figure 3. Changes in photophysical property and morphology of **BD-PG_{Me}/P₈** nanoplates upon stimuli-triggered “**BD-PG_{Me}** to **BD-COO_{Me}**” conversion. (a) UV-visible absorption spectra of **BD-PG_{Me}** (4.0 μ M) in $\text{CH}_3\text{CN}/\text{H}_2\text{O}$ (10/1, v/v) upon incubation with OONO^- at different concentrations (0-1 equiv) for 1 min at 37 $^\circ\text{C}$. (b) HPLC chromatograms of **BD-PG_{Me}** without treatment of OONO^- (top); with OONO^- (1 equiv) treatment for 1 min at 37 $^\circ\text{C}$ (middle); and **BD-COOH_{Me}** only (bottom). (c) UV-visible absorption spectra of the aqueous solution of **BD-PG_{Me}/P₈** (0.1 g/L **P₈**; 2.0 μ M **BD-PG_{Me}**) upon incubation with OONO^- (5 equiv) for varying time intervals (0-10 min) at 37 $^\circ\text{C}$. (d) UV-visible absorption response of **BD-PG_{Me}/P₈** (0.1 g/L **P₈**; 2.0 μ M **BD-PG_{Me}**) towards various ROSs and some physiological nucleophiles (5 equiv for ClO^- and OONO^- ; 100 equiv for other species); inset shows optical photographs of **BD-PG_{Me}/P₈** solutions before and after OONO^- (5 equiv) treatment. (e) Cryo-TEM image, (f) TEM image, and (g) AFM image of **BD-PG_{Me}/P₈** nano-assemblies (2.0% dye content) upon incubation with OONO^- (5 equiv) for 30 min at 37 $^\circ\text{C}$. Inset of (3e) shows a high magnification cryo-TEM image of the region marked with a red rectangle. (h) UV-visible absorption spectra of aqueous solutions of **BD-PG_{Me}/P₈** (0.4 g/L **P₈**) with different **BD-PG_{Me}** contents (0.5-3.4%) upon incubation with OONO^- (5 equiv) for 30 min at 37 $^\circ\text{C}$. (i) UV-visible absorption spectra of two-fold serially diluted solutions of **BD-PG_{Me}/P₈** (0.4 g/L **P₈**; 3.4% dye content) upon incubation with OONO^- (5 equiv) for 30 min at 37 $^\circ\text{C}$.

We further investigated the OONO^- -triggered ester-to-carboxylate conversion of **BD-PG_{Me}/P₈** nanoplates in the aqueous milieu. As expected, upon addition of OONO^- (5 equiv), J-aggregated **BD-PG_{Me}** dyes were converted into non-stacked **BD-COO_{Me}** within 10 min, as evidenced from the emergence of a new absorption band of **BD-COO_{Me}** at approximately 655 nm and the gradual attenuation of the J-band at 788 nm (Figure 3c). Concomitantly, the color of the **BD-PG_{Me}/P₈** solutions changed obviously, as shown in the inset of Figure 3d. Compared with **BD-PG_{Me}** monomers in $\text{CH}_3\text{CN}/\text{H}_2\text{O}$ (10/1, v/v) mixture (Figure 3a), OONO^- -actuated ester-to-carboxylate conversion of the **BD-PG_{Me}/P₈** nanoplates was slower. We proposed that dense slip-packing of **BD-PG_{Me}** dyes within nano-assemblies should be responsible for the slower ester-to-carboxylate conversion. It was also demonstrated that the **BD-PG_{Me}/P₈** nanoplates are highly selective for OONO^- over other ROSs and several typical

physiological nucleophiles (Figures 3d and S12). Notably, in our previous report,³¹ the arylboronate group of a water-soluble BODIPY-based probe (P-HP-FR, similar to **BD-PG_{Me}**) was completely cleaved after 150 min incubation with H_2O_2 (200 equiv) in aqueous solution. However, no appreciable change in UV-visible absorption spectra was observed before 90 min incubation of **BD-PG_{Me}/P₈** nanoplates with H_2O_2 (200 equiv; Figure S13a). The deprotection was not yet finished upon incubation with a higher concentration of H_2O_2 (5000 equiv) over 150 min (Figure S13b). The slower reaction rate of J-aggregated **BD-PG_{Me}** within nano-assemblies further demonstrated that dense packing of dyes would slow down the ester-to-carboxylate conversion rate. The J-band of BODIPY dyes disappeared after OONO^- -triggered hydrophobic **BD-PG_{Me}** to ionic **BD-COO_{Me}** transition (Figure 3c), whereas the **BD-COO_{Me}** dye was not observed in the effluent following 24 hours of dialysis

of $\text{BD-COO}^-_{\text{Me}}/\text{P}_8$ solution via HPLC monitoring (data not shown), indicating that $\text{BD-COO}^-_{\text{Me}}$ and P_8 still remained in the form of nano-aggregates as also confirmed by DLS measurement (Figure S14).

Cryogenic transmission electron microscopy (cryo-TEM) was adopted to characterize the in-solution structures of the $\text{BD-COO}^-_{\text{Me}}/\text{P}_8$ nano-assemblies, and bundled nanorods of ~ 180 nm in length were observed (Figure 3e). In TEM and AFM measurements, similar bundled nanorods were observed, possessing the same shape but longer length as those observed by cryo-TEM (Figures 3f and 3g). Taking the same nanostructure morphologies into consideration, the longer size observed in TEM and AFM images should be attributed to drying of the nano-assemblies during sample preparation. To understand more about the formation mechanism of the unusual bundled nanorods, we prepared nano-assemblies of $\text{BD-COOH}_{\text{Me}}/\text{P}_8$ (denoted as $^*\text{BD-COOH}_{\text{Me}}/\text{P}_8$) via self-assembly of $\text{BD-COOH}_{\text{Me}}$ and P_8 directly in aqueous solution according to the same procedure as that used for $\text{BD-PG}_{\text{Me}}/\text{P}_8$ preparation. The morphology of $^*\text{BD-COOH}_{\text{Me}}/\text{P}_8$ nano-assemblies was investigated by TEM, and nanoparticles rather than nanorods were observed (Figure S15), indicating that bundled nanorods of $\text{BD-COO}^-_{\text{Me}}/\text{P}_8$ might evolve from $\text{BD-PG}_{\text{Me}}/\text{P}_8$ nanoplates in the presence of peroxyinitrite. As for $\text{BD-PG}_{\text{Me}}/\text{P}_{50}$ and $\text{BD-PG}_{\text{Me}}/\text{P}_{80}$ nano-assemblies, OONO^- -actuated BD-PG_{Me} to $\text{BD-COO}^-_{\text{Me}}$ conversions were faster than those of $\text{BD-PG}_{\text{Me}}/\text{P}_8$ (Figures 3c, S16, and S17). The converted $\text{BD-COO}^-_{\text{Me}}/\text{P}_{50}$ and $\text{BD-COO}^-_{\text{Me}}/\text{P}_{80}$ remained in the form of micellar structures owing to strong hydrophobic interactions between PCL segments with slight increment in size due to the hydrophilic $\text{BD-COO}^-_{\text{Me}}$ dyes (Figure S18).

We further investigated OONO^- -actuated transformation behaviors of various $\text{BD-PG}_{\text{Me}}/\text{P}_8$ (0.4 g/L P_8) solutions with BD-PG_{Me} loading content from 0.5% to 3.4%, wherein BD-PG_{Me} dyes adopted a slip-stacked arrangement (Figure 2h). With regard to $\text{BD-PG}_{\text{Me}}/\text{P}_8$ nano-assemblies with dye content below 2.0%, only the monomer band at 655 nm was observed in UV-visible absorption spectra after OONO^- (5 equiv) treatment, confirming that all OONO^- -converted $\text{BD-COO}^-_{\text{Me}}$ dyes were dispersed in a non-stacked form (Figure 3h). When the dye content increased to 3.4%, another absorption band emerged at 740 nm after OONO^- (5 equiv) incubation, which should be ascribed to the J-aggregates of $\text{BD-COO}^-_{\text{Me}}$ dyes (Figure 3h). The change in the UV-visible absorption spectra of the OONO^- -converted $\text{BD-COO}^-_{\text{Me}}/\text{P}_8$ (3.4% dye content) solution was negligible following four 2-fold serial dilutions with PBS (Figure S19), demonstrating that the $\text{BD-COO}^-_{\text{Me}}$ J-aggregates were stable in water even after 1/16 dilution and thus should be located within the $\text{BD-COO}^-_{\text{Me}}/\text{P}_8$ nano-assemblies. Moreover, two-fold serially diluted $\text{BD-PG}_{\text{Me}}/\text{P}_8$ (3.4% dye content) solutions (i.e., 1/2, 1/4, and 1/8 dilutions) were prepared and treated with OONO^- (5 equiv). Both monomer and aggregate bands were observed in UV-visible absorption spectra with the ratio of two absorption bands comparable to that of the original solution (Figure 3i), suggesting that the dye rearrangement occurred within the nano-assemblies. Having established that OONO^- at low concentration could induce a rapid rearrangement of J-stacked BODIPY dyes within nano-assemblies in water, with remarkable photophysical changes, we then sought to apply our insights to the development of new stimuli-sensitive photofunctional tools applicable to living systems.

Stimuli-activatable nano-photosensitizers for specific photodynamic therapy. Benefiting from their excellent environmental stability, large extinction coefficients, facile modifications, and low dark toxicities, iodo-substituted BODIPY derivatives are emerging as ideal photosensitizers (PSs) to convert molecular oxygen to singlet oxygen ($^1\text{O}_2$) upon light irradiation for photodynamic therapy (PDT).^{9,55-58} However, low selectivity of the photosensitizers currently available for clinical PDT causes nonspecific photodamage to nearby healthy tissues, as well as prolonged skin injury.⁵⁹ Targeted activation enables the activatable photosensitizers to distinguish healthy from diseased cells, reducing nonspecific damage to adjacent healthy cells.³⁹⁻⁴² Since the slip-stacked BODIPY dye templated $\text{BD-PG}_{\text{Me}}/\text{P}_8$ nanoplates can act as an aqueous reservoir of PS and exhibit dramatic spectroscopic responses to external stimuli, the potential exists to selectively modulate the photosensitivity of $\text{BD-PG}_{\text{Me}}/\text{P}_8$ nanoplates in response to specific stimuli. A water-soluble 1,3-diphenylisobenzofuran derivative (QDPBF) was employed as an indicator to evaluate the $^1\text{O}_2$ generation.⁶⁰ Negligible change in QDPBF absorption was observed within the aqueous solution of $\text{BD-PG}_{\text{Me}}/\text{P}_8$ (0.05 g/L P_8 , 1.0 μM BD-PG_{Me}) either in darkness (Figure S22), or upon light irradiation at 655 nm (5 mW/cm²; Figure 4a), indicating that the photosensitivity of $\text{BD-PG}_{\text{Me}}/\text{P}_8$ nanoplates in producing $^1\text{O}_2$ was well suppressed. Encouragingly, the quenched photosensitivity of $\text{BD-PG}_{\text{Me}}/\text{P}_8$ nanoplates (hereafter denoted as $^{\text{nano}}\text{PS-PG}$) is a desirable feature as it meets the criteria for the off state of an activatable photosensitizer.

Gratifyingly, for the OONO^- (5.0 μM) converted $\text{BD-COO}^-_{\text{Me}}/\text{P}_8$ solution (hereafter denoted as $^{\text{nano}}\text{PS}$), significant decrease in QDPBF absorption was observed under light irradiation at 655 nm (5 mW/cm²) as shown in Figure 4b, demonstrating an effective $^1\text{O}_2$ generation. The change in absorbance of QDPBF (ΔAbs) at 412 nm was recorded at 10-s intervals to evaluate the photosensitivity with respect to producing $^1\text{O}_2$. In comparison, the ΔAbs of $^{\text{nano}}\text{PS}$ increased much more rapidly than that of $^{\text{nano}}\text{PS-PG}$ (Figure 4c). The ΔAbs of $^{\text{nano}}\text{PS}$ within 90s is comparable to that of $\text{BD-COO}^-_{\text{Me}}$ monomers and 15.9-fold greater than that of $^{\text{nano}}\text{PS-PG}$ (Figure 4d), suggesting an “off-on” response in the photoinduced singlet oxygen generation process, thus demonstrating the effectiveness of the slip-stacked dye arrangement in photosensitivity quenching and the stimuli-triggered restoring process. For quantitative evaluation, relative $^1\text{O}_2$ quantum yield (Φ_{Δ}) was determined by using methylene blue (MB) as a reference, and the Φ_{Δ} values of $^{\text{nano}}\text{PS}$ and $^{\text{nano}}\text{PS-PG}$ in aqueous media were calculated as 0.49 and 0.03, respectively (Figure 4d). Thus, it is clear that OONO^- at relatively low concentration is capable of converting a J-aggregated-photosensitizers doped nanoplate ($^{\text{nano}}\text{PS-PG}$) with inhibited photosensitivity into an active nano-photosensitizer ($^{\text{nano}}\text{PS}$) that generates $^1\text{O}_2$ when photoirradiated within the therapeutic window (in this case at 655 nm).

To gain insights into the quenching mechanism of $^{\text{nano}}\text{PS-PG}$, the photosensitivities of BD-PG_{Me} and $\text{BD-COO}^-_{\text{Me}}$ in a DMSO/water (8/2, v/v) mixture were evaluated, wherein BODIPY dyes (1.0 μM) dissolved as monomers (Figures 2a and S20). As shown in Figure 4d, ΔAbs of $\text{BD-COO}^-_{\text{Me}}$ upon photoirradiation (655 nm, 5 mW/cm²) for 90 s was 4.6-fold greater than that of BD-PG_{Me} , probably due to the difference in electron-withdrawing capability of their *meso*-substituents.³¹ The ΔAbs of slip-stacked BD-PG_{Me} ($^{\text{nano}}\text{PS-PG}$) upon photoirradiation was found to be approximately 25% that of the BD-PG_{Me} monomer, suggesting an inhibition of photosensitivity induced

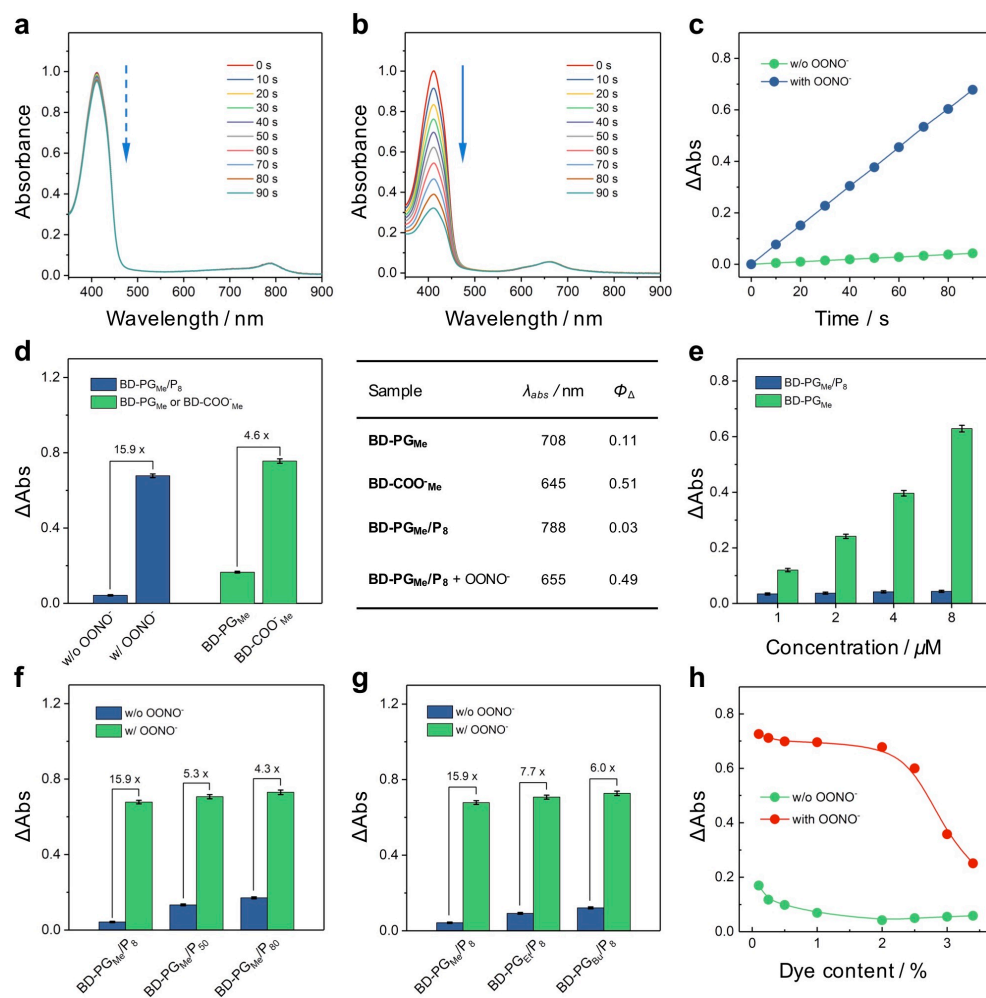


Figure 4. Inhibition and stimuli-triggered recovery of the photosensitivity of BODIPYs in nano-assemblies. (a,b) UV-visible absorption spectra of QDPBF upon light irradiation in the presence of (a) untreated or (b) OONO⁻-treated solution of **BD-PG_{Me}/P₈** for varying time intervals (0-90 s) at 37 °C. (c) Plots of change in absorbance (Δ Abs) of QDPBF at 412 nm upon light irradiation for different time intervals in the presence of untreated (green) or OONO⁻-treated (steel blue) solution of **BD-PG_{Me}/P₈** at 37 °C. (d) Δ Abs of QDPBF at 412 nm upon light irradiation for 90 s in the presence of **BD-PG_{Me}/P₈** (steel blue) without or with OONO⁻ pretreatment, or BODIPY monomers (**BD-PG_{Me}** or **BD-COO⁻Me**; green). Data of absorption maximum (λ_{abs}) and ¹O₂ quantum yields (Φ_{Δ}) are listed. (e) Δ Abs of QDPBF at 412 nm upon light irradiation for 60 s in the presence of **BD-PG_{Me}** (green) or **BD-PG_{Me}/P₈** (steel blue) at different concentrations of **BD-PG_{Me}** (1.0-8.0 μ M). (f-h) Δ Abs of QDPBF at 412 nm upon light irradiation for 90 s (f) in the presence of **BD-PG_{Me}/P₈**, **BD-PG_{Me}/P₅₀**, or **BD-PG_{Me}/P₈₀** without (steel blue) or with (green) OONO⁻ pretreatment, (g) in the presence of **BD-PG_{Me}/P₈**, **BD-PG_{Et}/P₈**, or **BD-PG_{Bu}/P₈** without (steel blue) or with (green) OONO⁻ pretreatment, (h) in the presence of **BD-PG_{Me}/P₈** (1.0 μ M **BD-PG_{Me}**) with different **BD-PG_{Me}** contents (0.5-3.4%) without (green) or with (red) OONO⁻ pretreatment. Light source used in above experiments is a laser (655 nm, 5 mW/cm²). Conc. 1.0 μ M **BD-PG_R**; 0.05 g/L **P_n** unless otherwise specified. As for (c-h), results represent the average of three independent experiments, and error bars represent mean \pm SD.

by intermolecular J-stacking (Figure 4d). In addition, Δ Abs of **BD-PG_{Me}** monomer upon photoirradiation was found to be increased with dye concentration in the range of 1.0-8.0 μ M, while for slip-stacked **BD-PG_{Me}** (^{nano}PS-PG), Δ Abs was almost irrespective of dye concentration (Figure 4e), indicating that the photosensitivity of ^{nano}PS-PG at 655 nm was completely suppressed as a result of the J-stacking arrangement of **BD-PG_{Me}** dyes. Further studies on the photosensitivities of various **BD-PG_{Me}/P_n** (**BD-PG_{Me}/P₅₀**, **BD-PG_{Me}/P₈₀**; Figures 4f and S23a) and **BD-PG_R/P₈** (**BD-PG_{Et}/P₈**, **BD-PG_{Bu}/P₈**; Figures 4g and S24a) nano-assemblies indicated that the efficiency of photosensitivity inhibition increased with the fractions of J-aggregated BODIPY dyes (α_j). Meanwhile, OONO⁻ pretreated samples (i.e., **BD-COO⁻Me/P₅₀**, **BD-COO⁻Me/P₈₀**, **BD-COO⁻Et/P₈**, and **BD-COO⁻Bu/P₈**) with non-stacked dye arrangements as

confirmed by the exclusively monomeric bands in UV-visible absorption spectra (Figures S16 and S21) all present strong photosensitivities comparable to that of ^{nano}PS (Figures 4f, 4g, S23b, and S24b).

We also evaluated the photosensitivities of **BD-PG_{Me}/P₈** solutions with different dye contents from 0.1% to 3.4% (Figures 4h and S25). Regarding **BD-PG_{Me}/P₈** solutions without OONO⁻ incubation, the photosensitivities were well suppressed, and the efficiency of inhibition was dependent on the fractions of J-aggregated dyes (α_j). Upon treatment with OONO⁻, photosensitivity of the stimuli-converted **BD-COO⁻Me/P₈** solutions was significantly enhanced, as shown in Figure 4h. The photosensitivities of **BD-COO⁻Me/P₈** solutions with dye contents in the range of 0.1-2.0% were comparable to that of **BD-COO⁻Me** monomer owing to the non-stacked arrangement of **BD-COO⁻Me** dyes. As

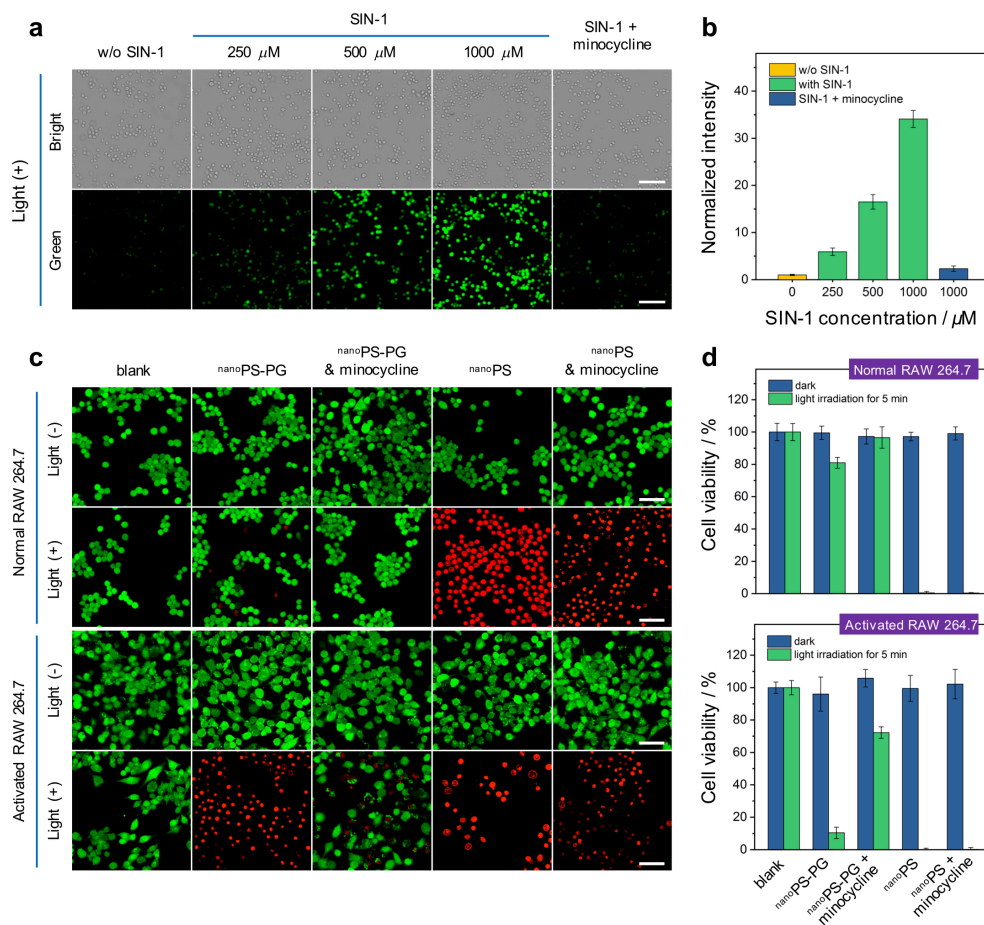


Figure 5. Intracellular $^1\text{O}_2$ production and cell viability assay. (a) Intracellular singlet oxygen ($^1\text{O}_2$) production using $^1\text{O}_2$ probe DCF-DA. RAW 264.7 cells were treated with nanoPS-PG for 30 min, and incubated with SIN-1 at different concentrations (first column: without SIN-1; second-fourth columns: 250, 500, 1000 μM SIN-1; last column: 1000 μM SIN-1 and 100 μM minocycline) for 2 h, then stained with 10.0 μM DCF-DA for 20 min. The cells were then subjected to light irradiation for 5 min and imaged. Scale bar is 100 μm . (b) Normalized green channel emission intensities quantified from fluorescence images in (a). (c) Live/Dead staining images of normal (top two lines) and activated (bottom two lines) RAW 264.7 cells. Cells were treated with different samples (first column: blank; second column: nanoPS-PG ; third column: nanoPS-PG and 100 μM minocycline; fourth column: nanoPS ; last column: nanoPS and 100 μM minocycline) for 2 h, and then subjected to light irradiation (second and last lines) or without light irradiation (top and third lines) for 5 min. After treatment, the cells were stained with 1.0 μM Calcein AM (live staining, green) and 6.0 μM PI (dead staining, red) for 20 min. Scale bar is 50 μm . (d) Cell viability of normal (top) or activated (bottom) RAW 264.7 cells treated at different conditions determined by MTT assay. Error bars represent mean \pm SD ($n = 5$). Light source used in above experiments is a red LED lamp (620-660 nm, 15 mW/cm 2). nanoPS-PG and nanoPS containing 1.0 μM BODIPY dyes were used in the above experiments.

for $\text{BD-COO}^-_{\text{Me}}/\text{P}_8$ solutions with dye contents beyond 2.0%, their photosensitivities were remarkably decreased due to the partial $\text{BD-COO}^-_{\text{Me}}$ J-aggregates located in the $\text{BD-COO}^-_{\text{Me}}/\text{P}_8$ nano-assemblies (Figure 3h), further demonstrating that the highly ordered J-stacking of dyes resulted in the inhibition of photosensitivity. Taken together, it was established that the photosensitivity of BODIPY dyes was governed by the dye arrangement within the nano-assemblies. Since $\text{BD-PG}_{\text{Me}}/\text{P}_8$ nanoplates with 2.0% dye content (denoted as nanoPS-PG) exhibited the largest off/on enhancement ratio, this sample was used in the following biological studies.

RAW 264.7 cells pretreated with or without SIN-1 (OONO^- donor 47) were incubated with nanoPS-PG for 2 h, following which the cells were washed. Upon imaging, fluorescence of nanoPS-PG was observed within cells indicating effective internalization (Figures S26a and S26b). To assess the effectiveness of intracellular OONO^- in activating our quenched nano-photo-

sensitizers (nanoPS-PG) after internalization, dichlorofluorescein diacetate (DCF-DA) was chosen as an oxidant-sensitive fluorescent probe to detect the formed singlet oxygen ($^1\text{O}_2$), which rapidly oxidize DCF-DA into highly fluorescent dichlorofluorescein (DCF). 61,62 As shown in Figure 5a, upon LED light irradiation (620-660 nm, 15 mW/cm 2), RAW 264.7 cells treated with nanoPS-PG and then DCF-DA showed negligible $^1\text{O}_2$ generation, which was reflected by the unobservable fluorescence intensity of DCF. A remarkable increase of DCF fluorescence was observed in cells pretreated with SIN-1 (OONO^- donor), and the enhancement in the fluorescence intensity was proportional to the dose of SIN-1 (250-1000 μM), suggesting that exogenous OONO^- apparently activated the potential nano-photosensitizers (Figures 5a and 5b). In contrast, the fluorescence signal related to DCF was significantly decreased by pretreating the cells with the OONO^- scavenger minocycline, 47 further verifying that exogenous OONO^- is the primary reason for intracellular activation of nanoPS-PG . It should be noted that the abovementioned RAW 264.7 cells in different experimental

groups all showed negligible fluorescence of DCF before photoirradiation (Figure S27), demonstrating that SIN-1 and its generated OONO^- did not interfere with the $^1\text{O}_2$ detection.

Encouraged by the above observations, the potential of $^{\text{nano}}\text{PS-PG}$ in response to endogenous OONO^- was evaluated in RAW 264.7 macrophages, which are known to release OONO^- upon stimulation with lipopolysaccharide (LPS)/interferon- γ (IFN- γ).⁶³ After demonstrating effective internalization of $^{\text{nano}}\text{PS-PG}$ into activated RAW 264.7 cells (Figure S26c), normal or activated RAW 264.7 macrophages (upon preincubation with LPS/IFN- γ for 20 h) were incubated with $^{\text{nano}}\text{PS-PG}$, then subjected to light irradiation (620–660 nm, 15 mW/cm²) for 5 min. After the light irradiation, cells were incubated at 37 °C (4 h for Live/Dead assay; 12 h for MTT assay), and the cell viability was assessed by using the Live/Dead cell viability assay with propidium iodide (PI) and Calcein AM (Figures 5c and S28), as well as MTT assay (Figure 5d). Only the activated RAW 264.7 cells pretreated with $^{\text{nano}}\text{PS-PG}$ were predominantly stained with PI, indicating selective photo-induction of cell death. Cell viability was positively correlated with $^{\text{nano}}\text{PS-PG}$ concentration and light irradiation dose (Figure S29a), but little cytotoxicity was observed among cells without light irradiation or normal RAW 264.7 cells treated with $^{\text{nano}}\text{PS-PG}$ (Figures 5c, 5d, and S29). Addition of OONO^- scavenger minocycline to the medium resulted in recovery of the viability of cells treated with $^{\text{nano}}\text{PS-PG}$ (Figures 5c, 5d, and S28), supporting the view that endogenous OONO^- selectively triggered the conversion of $^{\text{nano}}\text{PS-PG}$ into $^{\text{nano}}\text{PS}$ with an “off-on” activation of the photosensitivity, and thus induced cytotoxicity upon light irradiation. For further reference to confirm the mechanism, we also prepared $^{\text{nano}}\text{PS}$ by incubation of $^{\text{nano}}\text{PS-PG}$ with OONO^- , which has been proven to possess strong photosensitivity. After incubating RAW 264.7 cells with $^{\text{nano}}\text{PS}$, strong emissions were observed within cells, suggesting the internalization of $^{\text{nano}}\text{PS}$ into both normal and activated cells (Figure S30). Live/Dead staining and MTT assay clearly showed that both normal and activated RAW 264.7 cells treated with $^{\text{nano}}\text{PS}$ were completely killed upon light irradiation (620–660 nm, 15 mW/cm², 5 min), no matter whether or not they were pretreated with minocycline; meanwhile, cells without light irradiation appeared to suffer little damage (Figures 5c and 5d). Collectively, the above results suggest that $^{\text{nano}}\text{PS-PG}$ could serve as an endogenous OONO^- -activatable photosensitizer that targets cells or tissues with excessive peroxynitrite. Since OONO^- is known to be overproduced in atherosclerotic plaque-associated activated macrophages,^{64–66} $^{\text{nano}}\text{PS-PG}$ could be used as a promising activatable nano-photosensitizer for specific macrophage ablation in inflammatory atherosclerosis.

CONCLUSION

In summary, we established a versatile and robust strategy to manipulate water-stable J-aggregated dye templated nano-assemblies with stimuli-responsive photophysical properties, in addition to stability in cell culture medium through dyes-templated self-assembly of amphiphilic block copolymers. Following the strategy, a novel class of activatable nano-photosensitizers $\text{BD-PG}_{\text{Me}}/\text{P}_8$ was developed and exploited for targeted photodynamic ablation of activated RAW 264.7 macrophages with excessive endogenous peroxynitrite. The photosensitivity of BD-PG_{Me} was completely suppressed within $\text{BD-PG}_{\text{Me}}/\text{P}_8$ nanoplates due to strong π - π stacking interaction between slip-

stacked dyes. Upon incubation of $\text{BD-PG}_{\text{Me}}/\text{P}_8$ nano-assemblies with peroxynitrite at relatively low concentration, a rapid rearrangement of BODIPY dyes was established, leading to photosensitivity restoration. Since the mechanisms of stimuli-responsive photophysical and/or photochemical changes are based on the chemical structure transformation-induced dye rearrangement, they are not limited to the design of activatable nano-photosensitizers, but instead significantly expands the palette of design principles for photofunctional tools applicable to living systems, such as fluorogenic probes and ratiometric photoacoustic probes, among others, which could be prepared by facilely replacing the BODIPY-based photosensitizers adopted herein with other fluorophores or photoacoustic dyes as functional template dyes on demand. Moreover, the synthesis of carboxyl-caged dyes is flexible, thus allowing customization of diverse dye-templates sensitive to a broad range of biorelated species of interest via the introduction of specific triggering motifs. We envision that the scope and generality of slip-stacked dyes templated nano-assemblies with photophysical responses toward external stimuli would span far beyond the seminal example presented here.

ASSOCIATED CONTENT

Supporting Information

The Supporting Information is available free of charge on the ACS Publications website.

Experimental details, biological studies, supplementary figures, NMR and HRMS spectra (PDF)

AUTHOR INFORMATION

Corresponding Author

*chli@nankai.edu.cn

Notes

The authors declare no competing financial interest.

ACKNOWLEDGMENT

Financial support from National Natural Science Foundation of China (NSFC) projects (Grant no. 51673101 and 81601590), Natural Science Foundation of Tianjin of China (Grant no. 15JCZDJC65800), and the Fundamental Research Funds for Central Universities (China) is gratefully acknowledged.

REFERENCES

- (1) Würthner, F. Dipole-Dipole Interaction Driven Self-Assembly of Merocyanine Dyes: From Dimers to Nanoscale Objects and Supramolecular Materials. *Acc. Chem. Res.* **2016**, *49*, 868–876.
- (2) Würthner, F.; Kaiser, T. E.; Saha-Moller, C. R. J-Aggregates: From Serendipitous Discovery to Supramolecular Engineering of Functional Dye Materials. *Angew. Chem. Int. Ed.* **2011**, *50*, 3376–3410.
- (3) Eisele, D. M.; Knoester, J.; Kirstein, S.; Rabe, J. P.; Vanden Bout, D. A. Uniform Exciton Fluorescence from Individual Molecular Nanotubes Immobilized on Solid Substrates. *Nat. Nanotech.* **2009**, *4*, 658–663.
- (4) Eisele, D. M.; Cone, C. W.; Bloemsmas, E. A.; Vlaming, S. M.; Van der Kwaak, C. G. F.; Silbey, R. J.; Bawendi, M. G.; Knoester, J.; Rabe, J. P.; Vanden Bout, D. A. Utilizing Redox-Chemistry to Elucidate the Nature of Exciton Transitions in Supramolecular Dye Nanotubes. *Nat. Chem.* **2012**, *4*, 655–662.

- (5) Gauffrès, E.; Tang, N. Y.-W.; Lapointe, F.; Cabana, J.; Nadon, M.-A.; Cottenye, N.; Raymond, F.; Szkopek, T.; Martel, R. Giant Raman Scattering from J-Aggregated Dyes Inside Carbon Nanotubes for Multispectral Imaging. *Nat. Photon.* **2014**, *8*, 72-78.
- (6) Chen, Z.; Liu, Y.; Wagner, W.; Stepanenko, V.; Ren, X.; Ogi, S.; Würthner, F. Near-IR Absorbing J-Aggregate of an Amphiphilic BF₂-Azadipyromethene Dye by Kinetic Cooperative Self-Assembly. *Angew. Chem. Int. Ed.* **2017**, *56*, 5729-5733.
- (7) Cheung, S.; O'Shea, D. F. Directed Self-Assembly of Fluorescence Responsive Nanoparticles and Their Use for Real-Time Surface and Cellular Imaging. *Nat. Commun.* **2017**, *8*, 1885.
- (8) Gorl, D.; Zhang, X.; Würthner, F. Molecular Assemblies of Perylene Bisimide Dyes in Water. *Angew. Chem. Int. Ed.* **2012**, *51*, 6328-6348.
- (9) He, H.; Ji, S.; He, Y.; Zhu, A.; Zou, Y.; Deng, Y.; Ke, H.; Yang, H.; Zhao, Y.; Guo, Z.; Chen, H. Photoconversion-Tunable Fluorophore Vesicles for Wavelength-Dependent Photoinduced Cancer Therapy. *Adv. Mater.* **2017**, *29*, 1606690.
- (10) Ng, K. K.; Shakiba, M.; Huynh, E.; Weersink, R. A.; Roxin, Á.; Wilson, B. C.; Zheng, G. Stimuli-Responsive Photoacoustic Nanoswitch for In Vivo Sensing Applications. *ACS Nano* **2014**, *8*, 8363-8373.
- (11) Tian, D.; Qi, F.; Ma, H.; Wang, X.; Pan, Y.; Chen, R.; Shen, Z.; Liu, Z.; Huang, L.; Huang, W. Domino-Like Multi-Emissions Across Red and Near Infrared from Solid-State 2-/2,6-Aryl Substituted BODIPY Dyes. *Nat. Commun.* **2018**, *9*, 2688.
- (12) Yagai, S.; Okamura, S.; Nakano, Y.; Yamauchi, M.; Kishikawa, K.; Karatsu, T.; Kitamura, A.; Ueno, A.; Kuzuhara, D.; Yamada, H.; Seki, T.; Ito, H. Design Amphiphilic Dipolar π -Systems for Stimuli-Responsive Luminescent Materials Using Metastable States. *Nat. Commun.* **2014**, *5*, 4013.
- (13) Patalag, L. J.; Ho, L. P.; Jones, P. G.; Werz, D. B. Ethylene-Bridged Oligo-BODIPYs: Access to Intramolecular J-Aggregates and Superfluorophores. *J. Am. Chem. Soc.* **2017**, *139*, 15104-15113.
- (14) Biswas, S.; Ahn, H.; Bondar, M. V.; Belfield, K. D. Two-Photon Absorption Enhancement of Polymer-Templated Porphyrin-Based J-Aggregates. *Langmuir* **2012**, *28*, 1515-1522.
- (15) Kim, O.; Je, J.; Jernigan, G.; Buckley, L.; Whitten, D. Super-Helix Formation Induced by Cyanine J-aggregates onto Random-Coil Carboxymethyl Amylose as Template. *J. Am. Chem. Soc.* **2006**, *128*, 510-516.
- (16) Koti, A. S. R.; Periasamy, N. Self-Assembly of Template-Directed J-Aggregates of Porphyrin. *Chem. Mater.* **2003**, *15*, 369-371.
- (17) Weingarten, A. S.; Kazantsev, R. V.; Palmer, L. C.; McClendon, M. T.; Koltonow, A. R.; Samuel, A. P. S.; Kiebal, D. J.; Wasielewski, M. R.; Stupp, S. I. Self-Assembling Hydrogel Scaffolds for Photocatalytic Hydrogen Production. *Nat. Chem.* **2014**, *6*, 964-970.
- (18) Weingarten, A. S.; Kazantsev, R. V.; Palmer, L. C.; Fairfield, D. J.; Koltonow, A. R.; Stupp, S. I. Supramolecular Packing Controls H₂ Photocatalysis in Chromophore Amphiphile Hydrogels. *J. Am. Chem. Soc.* **2015**, *137*, 15241-15246.
- (19) Hestand, N. J.; Kazantsev, R. V.; Weingarten, A. S.; Palmer, L. C.; Stupp, S. I.; Spano, F. C. Extended-Charge-Transfer Excitons in Crystalline Supramolecular Photocatalytic Scaffolds. *J. Am. Chem. Soc.* **2016**, *138*, 11762-11774.
- (20) Harutyunyan, B.; Dannenhoffer, A. J.; Kewalramani, S.; Aytun, T.; Fairfield, D. J.; Stupp, S. I.; Bedzyk, M. J. Molecular Packing of Amphiphilic Nanosheets Resolved by X-ray Scattering. *J. Phys. Chem. C* **2017**, *121*, 1047-1054.
- (21) Kazantsev, R. V.; Dannenhoffer, A. J.; Weingarten, A. S.; Phelan, B. T.; Harutyunyan, B.; Aytun, T.; Narayanan, A.; Fairfield, D. J.; Boekhoven, J.; Sai, H.; Senesi, A.; O'Dogherty, P. I.; Palmer, L. C.; Bedzyk, M. J.; Wasielewski, M. R.; Stupp, S. I. Crystal-Phase Transitions and Photocatalysis in Supramolecular Scaffolds. *J. Am. Chem. Soc.* **2017**, *139*, 6120-6127.
- (22) Kazantsev, R. V.; Dannenhoffer, A. J.; Aytun, T.; Harutyunyan, B.; Fairfield, D. J.; Bedzyk, M. J.; Stupp, S. I. Molecular Control of Internal Crystallization and Photocatalytic Function in Supramolecular Nanostructures. *Chem.* **2018**, *4*, 1596-1608.
- (23) Karton-Lifshin, N.; Segal, E.; Omer, L.; Portnoy, M.; Satchi-Fainaro, R.; Shabat, D. A Unique Paradigm for a Turn-ON Near-Infrared Cyanine-Based Probe: Noninvasive Intravital Optical Imaging of Hydrogen Peroxide. *J. Am. Chem. Soc.* **2011**, *133*, 10960-10965.
- (24) Wu, H.; Alexander, S. C.; Jin, S.; Devaraj, N. K. A Bioorthogonal Near-Infrared Fluorogenic Probe for mRNA Detection. *J. Am. Chem. Soc.* **2016**, *138*, 11429-11432.
- (25) Lincoln, R.; Greene, L. E.; Zhang, W.; Louisia, S.; Cosa, G. Mitochondria Alkylation and Cellular Trafficking Mapped with a Lipophilic BODIPY-Acrolein Fluorogenic Probe. *J. Am. Chem. Soc.* **2017**, *139*, 16273-16281.
- (26) Lin, V. S.; Chen, W.; Xian, M.; Chang, C. J. Chemical Probes for Molecular Imaging and Detection of Hydrogen Sulfide and Reactive Sulfur Species in Biological Systems. *Chem. Soc. Rev.* **2015**, *44*, 4596-4618.
- (27) Chan, J.; Dodani, S. C.; Chang, C. J. Reaction-Based Small-Molecule Fluorescent Probes for Chemoselective Bioimaging. *Nat. Chem.* **2012**, *4*, 973-984.
- (28) Umezawa, K.; Yoshida, M.; Kamiya, M.; Yamasoba, T.; Urano, Y. Rational Design of Reversible Fluorescent Probes for Live-Cell Imaging and Quantification of Fast Glutathione Dynamics. *Nat. Chem.* **2017**, *9*, 279-286.
- (29) Asanuma, D.; Sakabe, M.; Kamiya, M.; Yamamoto, K.; Hiratake, J.; Ogawa, M.; Kosaka, N.; Choyke, P. L.; Nagano, T.; Kobayashi, H.; Urano, Y. Sensitive β -Galactosidase-Targeting Fluorescence Probe for Visualizing Small Peritoneal Metastatic Tumours in Vivo. *Nat. Commun.* **2015**, *6*, 6463.
- (30) Shieh, P.; Dien, V. T.; Beahm, B. J.; Castellano, J. M.; Wyss-Coray, T.; Bertozzi, C. R. CalFluors: A Universal Motif for Fluorogenic Azide Probes across the Visible Spectrum. *J. Am. Chem. Soc.* **2015**, *137*, 7145-7151.
- (31) Chen, H.; He, X.; Su, M.; Zhai, W.; Zhang, H.; Li, C. A General Strategy Toward Highly Fluorogenic Bioprobes Emitting across the Visible Spectrum. *J. Am. Chem. Soc.* **2017**, *139*, 10157-10163.
- (32) Zhang, J.; Zhen, X.; Upputuri, P. K.; Pramanik, M.; Chen, P.; Pu, K. Activatable Photoacoustic Nanoprobes for in Vivo Ratiometric Imaging of Peroxynitrite. *Adv. Mater.* **2017**, *29*, 1604764.
- (33) Reinhardt, C. J.; Zhou, E. Y.; Jorgensen, M. D.; Partipilo, G.; Chan, J. A Ratiometric Acoustogenic Probe for in Vivo Imaging of Endogenous Nitric Oxide. *J. Am. Chem. Soc.* **2018**, *140*, 1011-1018.
- (34) Li, H.; Zhang, P.; Smaga, L. P.; Hoffman, R. A.; Chan, J. Photoacoustic Probes for Ratiometric Imaging of Copper(II). *J. Am. Chem. Soc.* **2015**, *137*, 15628-15631.
- (35) Zheng, G.; Chen, J.; Stefflova, K.; Jarvi, M.; Li, H.; Wilson, B. C. Photodynamic Molecular Beacon as an Activatable Photosensitizer Based on Protease-Controlled Singlet Oxygen Quenching and Activation. *PNAS* **2007**, *104*, 8989-8994.
- (36) Chen, J.; Stefflova, K.; Niedre, M. J.; Wilson, B. C.; Chance, B.; Glickson, J. D.; Zheng, G. Protease-Triggered Photosensitizing Beacon Based on Singlet Oxygen Quenching and Activation. *J. Am. Chem. Soc.* **2004**, *126*, 11450-11451.
- (37) Clo', E.; Snyder, J. W.; Voigt, N. V.; Ogilby, P. R.; Gothelf, K. V. DNA-Programmed Control of Photosensitized Singlet Oxygen Production. *J. Am. Chem. Soc.* **2006**, *128*, 4200-4201.
- (38) Fan, H.; Yan, G.; Zhao, Z.; Hu, X.; Zhang, W.; Liu, H.; Fu, X.; Fu, T.; Zhang, X.; Tan, W. A Smart Photosensitizer-Manganese Dioxide Nanosystem for Enhanced Photodynamic Therapy by Reducing Glutathione Levels in Cancer Cells. *Angew. Chem. Int. Ed.* **2016**, *55*, 5477-5482.
- (39) Turan, I. S.; Cakmak, F. P.; Yildirim, D. C.; Cetin-Atalay, R.; Akkaya, E. U. Near-IR Absorbing BODIPY Derivatives as Glutathione-Activated Photosensitizers for Selective Photodynamic Action. *Chem. Eur. J.* **2014**, *20*, 16088-16092.
- (40) Piao, W.; Hanaoka, K.; Fujisawa, T.; Takeuchi, S.; Komatsu, T.; Ueno, T.; Terai, T.; Tahara, T.; Nagano, T.; Urano, Y. Development of an Azo-Based Photosensitizer Activated under Mild Hypoxia for Photodynamic Therapy. *J. Am. Chem. Soc.* **2017**, *139*, 13713-13719.
- (41) Park, W.; Park, S.; Cho, S.; Shin, H.; Jung, Y.; Lee, B.; Na, K.; Kim, D. Intermolecular Structural Change for Thermoswitchable Polymeric Photosensitizer. *J. Am. Chem. Soc.* **2016**, *138*, 10734-10737.

(42) Lovell, J. F.; Liu, T. W. B.; Chen, J.; Zheng, G. Activatable Photosensitizers for Imaging and Therapy. *Chem. Rev.* **2010**, *110*, 2839-2857.

(43) Durantini, A. M.; Greene, L. E.; Lincoln, R.; Martínez, S. R.; Cosa, G. Reactive Oxygen Species Mediated Activation of a Dormant Singlet Oxygen Photosensitizer: From Autocatalytic Singlet Oxygen Amplification to Chemically Controlled Photodynamic Therapy. *J. Am. Chem. Soc.* **2016**, *138*, 1215-1225.

(44) Yuan, Y.; Zhang, C.; Gao, M.; Zhang, R.; Tang, B. Z.; Liu, B. Specific Light-Up Bioprobe with Aggregation-Induced Emission and Activatable Photoactivity for the Targeted and Image-Guided Photodynamic Ablation of Cancer Cells. *Angew. Chem. Int. Ed.* **2014**, *53*, 1780-1786.

(45) Qi, J.; Chen, C.; Zhang, X.; Hu, X.; Ji, S.; Kwok, R. T.K.; Lam, J. W.Y.; Ding, D.; Tang, B. Z. Light-driven Transformable Optical Agent with Adaptive Functions for Boosting Cancer Surgery Outcomes. *Nat. Commun.* **2018**, *9*, 1848.

(46) Helms, V. Principles of Computational Cell Biology, Wiley-VCH, **2008**.

(47) Jia, X.; Chen, Q.; Yang, Y.; Tang, Y.; Wang, R.; Xu, Y.; Zhu, W.; Qian, X. FRET-Based Mito-Specific Fluorescent Probe for Ratiometric Detection and Imaging of Endogenous Peroxynitrite: Dyad of Cy3 and Cy5. *J. Am. Chem. Soc.* **2016**, *138*, 10778-10781.

(48) Escudero, D. Revising Intramolecular Photoinduced Electron Transfer (PET) from First-Principles. *Acc. Chem. Res.* **2016**, *49*, 1816-1824.

(49) Grossi, M.; Morgunova, M.; Cheung, S.; Scholz, D.; Conroy, E.; Terrile, M.; Panarella, A.; Simpson, J. C.; Gallagher, W. M.; O'Shea, D. F. Lysosome Triggered Near-Infrared Fluorescence Imaging of Cellular Trafficking Processes in Real Time. *Nat. Commun.* **2016**, *7*, 10855.

(50) Choi, S.; Bouffard, J.; Kim, Y. Aggregation-Induced Emission Enhancement of a *meso*-Trifluoromethyl BODIPY via J-Aggregation. *Chem. Sci.* **2014**, *5*, 751-755.

(51) Kubota, Y.; Tsuzuki, T.; Funabiki, K.; Ebihara, M.; Matsui, M. Synthesis and Fluorescence Properties of a Pyridomethene-BF₂ Complex. *Org. Lett.* **2010**, *12*, 4010-4013.

(52) Manzano, H.; Esnal, I.; Marqués-Matesanz, T.; Bañuelos, J.; López-Arbeloa, I.; Ortiz, M. J.; Cerdán, L.; Costela, A.; García-Moreno, I.; Chiara, J. L. Unprecedented J-Aggregated Dyes in Pure Organic Solvents. *Adv. Funct. Mater.* **2016**, *26*, 2756-2769.

(53) Yuan, K.; Wang, X.; Møllerup, S. K.; Kozin, I.; Wang, S. Spiro-BODIPYs with a Diaryl Chelate: Impact on Aggregation and Luminescence. *J. Org. Chem.* **2017**, *82*, 13481-13487.

(54) Kim, J.; Park, J.; Lee, H.; Choi, Y.; Kim, Y. A Boronate-Based Fluorescent Probe for the Selective Detection of Cellular Peroxynitrite. *Chem. Commun.* **2014**, *50*, 9353-9356.

(55) Awuah, S. G.; You, Y. Boron Dipyrromethene (BODIPY)-Based Photosensitizers for Photodynamic Therapy. *RSC Adv.* **2012**, *2*, 11169-11183.

(56) Kamkaew, A.; Lim, S. H.; Lee, H. B.; Kiew, L. V.; Chung, L. Y.; Burgess, K. BODIPY Dyes in Photodynamic Therapy. *Chem. Soc. Rev.* **2013**, *42*, 77-88.

(57) Zhao, J.; Xu, K.; Yang, W.; Wang, Z.; Zhong, F. The Triplet Excited State of Bodipy: Formation, Modulation and Application. *Chem. Soc. Rev.* **2015**, *44*, 8904-8939.

(58) Huang, L.; Li, Z.; Zhao, Y.; Zhang, Y.; Wu, S.; Zhao, J.; Han, G. Ultralow-Power Near Infrared Lamp Light Operable Targeted Organic Nanoparticle Photodynamic Therapy. *J. Am. Chem. Soc.* **2016**, *138*, 14586-14591.

(59) O'Connor, A. E.; Gallagher, W. M.; Byrne, A. T. Porphyrin and Nonporphyrin Photosensitizers in Oncology: Preclinical and Clinical Advances in Photodynamic Therapy. *Photochem. Photobiol.* **2009**, *85*, 1053-1074.

(60) Amat-Guerri, F.; Lempe, E.; Lissi, E. A.; Rodriguez, F. J.; Trull, F. R. Water-Soluble 1,3-Diphenylisobenzofuran Derivatives Synthesis and Evaluation as Singlet Molecular Oxygen Acceptors for Biological Systems. *J. Photoch. Photobiol.* **1996**, *A93*, 49-56.

(61) Cheng, Y.; Cheng, H.; Jiang, C.; Qiu, X.; Wang, K.; Huan, W.; Yuan, A.; Wu, J.; Hu, Y. Perfluorocarbon Nanoparticles Enhance Reactive Oxygen Levels and Tumour Growth Inhibition in Photodynamic Therapy. *Nat. Commun.* **2015**, *6*, 8785.

(62) Idris, N. M.; Gnanasammandhan, M. K.; Zhang, J.; Ho, P. C.; Mahendran, R.; Zhang, Y. In Vivo Photodynamic Therapy Using Up-conversion Nanoparticles as Remote-Controlled Nanotransducers. *Nat. Med.* **2012**, *18*, 1580-1585.

(63) Kim, H.; Kim, Y.; Kim, I. H.; Kim, K.; Choi, Y. ROS-Responsive Activatable Photosensitizing Agent for Imaging and Photodynamic Therapy of Activated Macrophages. *Theranostics* **2014**, *4*, 1-11.

(64) Münzel, T.; Gori, T.; Bruno, R. M.; Taddei, S. Is Oxidative Stress a Therapeutic Target in Cardiovascular Disease? *Eur. Heart J.* **2010**, *31*, 2741-2749.

(65) McCarthy, J. R.; Korngold, E.; Weissleder, R.; Jaffer, F. A. A Light-Activated Theranostic Nanoagent for Targeted Macrophage Ablation in Inflammatory Atherosclerosis. *Small* **2010**, *6*, 2041-2049.

(66) McCarthy, J. R.; Jaffer, F. A.; Weissleder, R. A Macrophage-Targeted Theranostic Nanoparticle for Biomedical Applications. *Small* **2006**, *2*, 983-987.

